

Reaction Intermediates of Quinol Oxidation in a Photoactivatable System that Mimics Electron Transfer in the Cytochrome *bc*₁ Complex

Jonathan L. Cape,[†] Michael K. Bowman,^{†,‡} and David M. Kramer^{*,†}

Contribution from the Institute of Biological Chemistry, Washington State University, 289 Clark Hall, Pullman, Washington 99164-6314 and Structural Biology and Microimaging, Battelle Northwest Laboratories, Richland, Washington 99352-0999

Received October 4, 2004; E-mail: dkramer@wsu.edu

Abstract: Current competing models for the two-electron oxidation of quinol (QH₂) at the cytochrome *bc*₁ complex and related complexes impose distinct requirements for the reaction intermediate. At present, the intermediate species of the enzymatic oxidation process have not been observed or characterized, probably due to their transient nature. Here, we use a biomimetic oxidant, excited-state Ru(bpy)₂(pbim)⁺ (bpy = 2,2'-dipyridyl, pbim = 2-(2-pyridyl)benzimidazole) in an aprotic medium to probe the oxidation of the ubiquinol analogue, 2,3-dimethoxy-5-methyl-1,4-benzoquinol (UQH₂-0), and the plastoquinol analogue, trimethyl-1,4-benzoquinol (TMQH₂-0), using time-resolved and steady-state spectroscopic techniques. Despite its simplicity, this system qualitatively reproduces key features observed during ubiquinol oxidation by the mitochondrial cytochrome *bc*₁ complex. Comparison of isotope-dependent activation properties in the native and synthetic systems as well as analysis of the time-resolved direct-detection electron paramagnetic resonance signals in the synthetic system allows us to conclude that (1) the initial and rate-limiting step in quinol oxidation, both in the biological and biomimetic systems, involves electron and proton transfer, probably via a proton-coupled electron-transfer mechanism, (2) a neutral semiquinone intermediate is formed in the biomimetic system, and (3) oxidation of the QH[•]/QH₂ couple for UQH₂-0, but not TMQH₂-0, exhibits an unusual and unexpected primary deuterium kinetic isotope effect on its Arrhenius activation energy ($\Delta G^{\ddagger S}$), where $\Delta G^{\ddagger S}$ for the protiated form is larger than that for the deuterated form. The same behavior is observed during steady-state turnover of the cyt *bc*₁ complex using ubiquinol, but not plastoquinol, as a substrate, leading to the conclusion that similar chemical pathways are involved in both systems. The synthetic system is an unambiguous *n* = 1 electron acceptor, and it is thus inferred that sequential oxidation of ubiquinol (by two sequential *n* = 1 processes) is more rapid than a truly concerted (*n* = 2) oxidation in the cyt *bc*₁ complex.

Introduction

Quinone (Q) and quinol (QH₂) species play central roles in energy transduction for a broad range of species in all phylogenetic branches of life, from Archae and Eubacteria to Eukaryotes.^{1–3} The most commonly recognized function of biological Q/QH₂ species is to shuttle electrons between the various membrane-bound components of electron-transport chains while generating a proton motive force through the uptake and release of protons on opposite sides of the membrane.^{1,3,4}

The reactions of Q and QH₂ species in biological electron-transport chains involve a transition at several points between the two-electron (*n* = 2) redox chemistry of the Q/QH₂ couple and *n* = 1 chemistry of transition-metal and organic cofactors

in electron-transport enzymes. This transition typically leads to the transient formation of semiquinone (SQ) radicals that can potentially react with oxygen,^{5–8} eventually forming damaging reactive oxygen species.^{9–11} To minimize such side reactions, electron-transfer (ET) proteins strictly control the redox reactions of Q/QH₂ couples or otherwise shield them from interactions with O₂. Failure to prevent the reduction of oxygen by SQ radicals can result in oxidative stress and tissue damage.^{12–16}

[†] Washington State University.

[‡] Battelle Northwest Laboratories.

- (1) *Coenzyme Q: Biochemistry, Bioenergetics, and Clinical Applications of Ubiquinone*; Wiley: New York, 1985.
- (2) Saul, P. *The Chemistry of Quinoid Compounds*; Interscience: New York, 1974.
- (3) Cramer, W. A.; Knaff, D. B. *Function of Quinones in Energy Conserving Systems*; 1982.
- (4) Nohl, H.; Gille, L.; Staniek, K. *Ann. N.Y. Acad. Sci.* **1998**, *854*, 394–409.

- (5) Roginsky, V. A.; Barsukova, T. *Perkin Trans. 2* **2000**, 1575–1582.
- (6) Kantilal, P. B.; Willson, R. L. *J. Chem. Soc., Faraday Trans. 1* **1973**, 814–825.
- (7) Demin, O. V.; Kholodenko, B. N.; Skulachev, V. P. *Mol. Cell. Biochem.* **1998**, *184*, 21–33.
- (8) Kozlov, A. V.; Nohl, H.; Gille, L. *Bioorg. Chem.* **1998**, *26*, 334–344.
- (9) Muller, F.; Roberts, A. G.; Bowman, M. K.; Kramer, D. M. *Biochemistry* **2003**, *42*, 6493–6499.
- (10) Muller, F.; Crofts, A. R.; Kramer, D. M. *Biochemistry* **2002**, *41*, 7866–7874.
- (11) Kramer, D. M.; Roberts, A. G.; Muller, F.; Cape, J.; Bowman, M. K. *Methods Enzymol.* **2004**, *382*, 21–45.
- (12) Panaretakis, T.; Shabalina, I. G.; Grandier, D.; Shoshan, M. C.; DePierre, J. W. *Toxicol. Appl. Pharmacol.* **2001**, *173*, 56–64.
- (13) Papa, S.; Skulachev, V. P. *Mol. Cell. Biochem.* **1997**, *174*, 305–319.
- (14) Petrosillo, G.; Ruggiero, F. M.; Paradies, G. *FASEB J.* **2003**, *17*, 2202–2208.

In this context, the control of ubiquinol (UQH₂) oxidation at the quinol oxidation (Q_o) binding site of the cyt *bc*₁ complex is of particular interest due to its potential as a site for superoxide production in mitochondria under both pathological¹⁷ and partially inhibited conditions.^{9,10} This reaction is a key step in the catalytic cycle of the complex, called the modified Q-cycle,^{18,19} whereby the UQH₂ is oxidized in an unusual ‘bifurcated’ electron-transfer (ET) mechanism with one electron reducing a high-potential ‘Rieske’ [2Fe2S] cluster²⁰ while the other electron reduces a low-potential cyt *b* heme (*b*_L). In the case of the mitochondrial form of the enzyme, the high-potential redox chain (consisting of the Rieske [2Fe2S] cluster and cyt *c*₁) directs electrons derived from quinol oxidation at the Q_o site to a mobile *c*-type cytochrome, which eventually reduces cytochrome *c* oxidase. The ‘low-potential chain’ consists of a ubiquinone reductase (Q_i) site, located on the opposite side of the membrane from the Q_o site, and two cyt *b* hemes (cyt *b*_L and *b*_H) that span the membrane, connecting the two sites. Two turnovers of the Q_o site result in the electrogenic accumulation of two electrons on the low-potential chain, eventually reducing a UQ to UQH₂ at the Q_i site. The net result of the Q-cycle mechanism is an increase in the proton-pumping efficiency of the cyt *bc*₁ complex through recycling of electrons to the Q_i site and re-reduction of the quinone pool.

A major question about the Q-cycle is how ET bifurcation is enforced by the cyt *bc*₁ complex while the thermodynamically favored bypass reactions of quinol oxidation intermediates are blocked, including those resulting in superoxide production, which would be expected to occur with a reactive SQ intermediate.^{9–11} Models that explain this behavior can be divided into two general categories.^{19,21–27} In (what we will term) ‘Type I’ models, QH₂ is oxidized by two sequential *n* = 1 electron transfers, producing a transient SQ intermediate that is either thermodynamically stabilized²⁷ or kinetically steered^{19,21,22,24} (via cyt *b*_L reduction) to prevent bypass reactions. ‘Type II’ models, also called double-concerted electron-transfer (DCET) models,^{23,28–31} invoke a truly concerted double-ET process, which simultaneously reduces the Rieske [2Fe2S] cluster and cyt *b*_L with no SQ intermediate. The lack of SQ effectively avoids bypass reactions. At present, no Q_o site semiquinone has been observed,³² but such negative results have been readily rationalized within either type of model.^{11,23,32,33}

In recent work³⁴ we attempted to test for the operation of Type I and II models by comparing the thermodynamic and kinetic properties of steady-state QH₂ oxidation by the cyt *bc*₁ complex for both the bifurcated reaction and the inhibitor-induced production of superoxide, which proceeds via *n* = 1 ET from QH₂ to the Rieske [2Fe2S] center, resulting in an O₂-reactive semiquinone intermediate.^{9–11} Our results showed virtually identical activation energy (ΔG^{TS}) values for UQH₂-10 oxidation occurring via the bifurcated reaction and inhibitor-induced superoxide production, regardless of the type of quinol substrate used. These results were interpreted as being incompatible with a Type II model since this model requires uninhibited and partially inhibited turnover to occur via different ET mechanisms with different TS energies:³⁵ uninhibited turnover involving direct conversion of QH₂ to Q and partially inhibited turnover producing a SQ that is oxidized to Q in subsequent reactions.

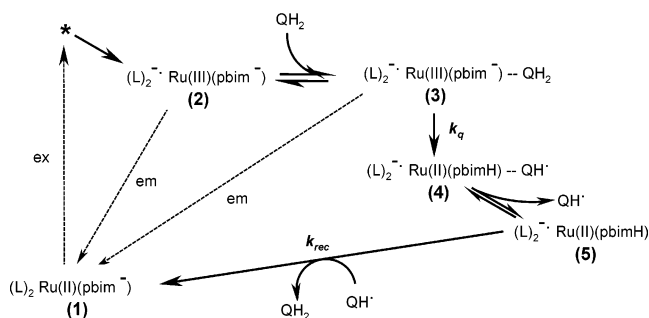
In addition, these studies revealed that the oxidation of UQH₂, but not other quinol substrates, by the cyt *bc*₁ complex exhibited an unusual isotope effect on the activation energy, where $\Delta G^{\text{TS}}(\text{D}) < \Delta G^{\text{TS}}(\text{H})$ by 20 kJ/mol. Remarkably, a similar ‘activation’ isotope effect has been observed in the oxidation of UQH₂-10 by α -tocopherol radical by Nagaoka and co-workers,³⁶ who reported $\Delta G^{\text{TS}}(\text{D}) < \Delta G^{\text{TS}}(\text{H})$ by ~ 5 kJ/mol (a 50% overall decrease in the slope of their Arrhenius plot when UQH₂ was deuterated in its hydroxyl positions). The effect was additionally sensitive to the type of quinol/hydrogen donors.³⁷ Although a definitive mechanism has not been assigned for this and other^{38–41} unexpected ‘activation’ isotope effects, we postulate that this rare effect might reflect an unusual, but not unprecedented, reaction coordinate for UQH₂ oxidation relative to other quinol oxidation reactions based on its observation in two different reaction systems. Using this approach we can test whether the unique activation isotope effect is indeed consistent with the one-electron oxidation of UQH₂ via a net hydrogen-transfer mechanism due to the improbability of both reactions sharing exactly the same reaction coordinate, thus discriminating between Type I and II mechanisms for the cyt *bc*₁ complex.

Toward addressing this issue, we demonstrate here the use of a photoactivatable ruthenium complex (see Scheme 1), Ru-(bpy)₂(pbim)⁺ (**1**) (bpy = 2,2′-dipyridyl; pbim = 2-(2-pyridyl)-benzimidazolone), that mimics the proton-coupled electron-transfer (PCET) reactivity^{42,43} and hydrogen-bonding ability^{44,45}

- (15) Suzuki, S.; Higuchi, M.; Proske, R. J.; Oridate, N.; Hong, W. K.; Lotan, R. *Oncogene* **1999**, *18*, 6380–6387.
 (16) Degli Esposti, M.; McLennan, H. *FEBS Lett.* **1998**, *430*, 338–342.
 (17) Petrosillo, G.; Ruggiero, F. M.; Di Venosa, N.; Paradies, G. *FASEB J.* **2003**, *17*, 714–716.
 (18) Crofts, A. R.; Meinhardt, S. W.; Jones, K. R.; Snozzi, M. *Biochim. Biophys. Acta* **1983**, *723*, 202–218.
 (19) Crofts, A. R.; Wang, Z. *Photosynth. Res.* **1989**, *22*.
 (20) Brugna, M.; Albouy, D.; Nitschke, W. *J. Bacteriol.* **1998**, *180*, 3719–3723.
 (21) Hong, S.; Ugulava, N.; Kuras-Guergova, M.; Crofts, A. R. *J. Biol. Chem.* **1999**, *274*, 33931–33944.
 (22) Crofts, A. R.; Shinkarev, V. P.; Kolling, D. R.; Hong, S. *J. Biol. Chem.* **2003**, *278*, 36191–36201.
 (23) Osyczka, A.; Moser, C. C.; Daldal, F.; Dutton, P. L. *Nature* **2004**, *427*, 607–612.
 (24) Rich, P. *Biochim. Biophys. Acta* **2004**, *1658*, 165–171.
 (25) Snyder, C. H.; Gutierrez-Cirlos, E. B.; Trumpower, B. L. *J. Biol. Chem.* **2000**, *275*, 13535–13541.
 (26) Berry, E. A.; Huang, L. S. *FEBS Lett.* **2003**, *555*, 13–20.
 (27) Link, T. A. *FEBS Lett.* **1997**, *412*, 257–264.
 (28) Trumpower, B. L. *Biochim. Biophys. Acta* **2002**, *1555*, 166–173.
 (29) Snyder, C.; Trumpower, B. L. *Biochim. Biophys. Acta* **1998**, *1365*, 125–134.
 (30) Yu, C. A.; Xia, D.; Kim, H.; Deisenhofer, J.; Zhang, L.; Kachurin, A. M.; Yu, L. *Biochim. Biophys. Acta* **1998**, *1365*, 151–158.
 (31) Yu, C. A.; Tian, H.; Zhang, L.; Deng, K. P.; Shenoy, S. K.; Yu, L.; Xia, D.; Kim, H.; Deisenhofer, J. *J. Bioenerg. Biomembr.* **1999**, *31*, 191–199.

- (32) Junemann, S.; Heathcote, P.; Rich, P. R. *J. Biol. Chem.* **1998**, *273*, 21603–21607.
 (33) Crofts, A. R.; Shinkarev, V. P.; Kolling, D. R.; Hong, S. *J. Biol. Chem.* **2003**, *278*, 36191–36201.
 (34) Kramer, D. M.; Cape, J.; Forquer, I.; Muller, F.; Bowman, M. K. *Biochemistry*, submitted for publication. (b) Forquer, I.; Cape, J.; Bowman, M. K.; Kramer, D. M. In *Photosynthesis: Fundamental Aspects to Global Perspectives*; van der Est, A., Bruce, D., Eds.; ACG Publishing: Lawrence, KA, 2005; in press. (c) Kramer, D.; Cape, J.; Bowman, M. K. In *Photosynthesis: Fundamental Aspects to Global Perspectives*; van der Est, A., Bruce, D., Eds.; ACG Publishing: Lawrence, KA, 2005; in press.
 (35) Zisman, L. D.; Beratan, D. N. *J. Chem. Phys.* **1996**, *105*, 165–176.
 (36) Nagaoka, S.-i.; Nishioku, Y.; Mukai, K. *Chem. Phys. Lett.* **1998**, *287*, 70–74.
 (37) Nagaoka, S.-i.; Inoue, M.; Nishioka, C.; Nishioku, Y.; Tsunoda, S.; Ohguchi, C.; Ohara, K.; Mulkai, K.; Nagashima, U. *J. Phys. Chem. B.* **2000**, *104*, 856–862.
 (38) Cheng, T.-Y.; Bullock, R. M. *J. Am. Chem. Soc.* **1999**, *121*, 3150–3155.
 (39) Koch, H. F.; Dahlberg, D. B.; McEntee, M. F.; Klecha, C. J. *J. Am. Chem. Soc.* **1976**, *98*, 1060–1061.
 (40) Melander, L.; Saunders, W. *Reaction Rates of Isotopic Molecules*; Wiley-Interscience: New York, 1980.
 (41) Willi, A. V.; Won, C. M. *J. Am. Chem. Soc.* **1968**, *90*, 5999–6001.
 (42) Kuila, D.; Fee, J. A. *J. Biol. Chem.* **1986**, *261*, 2768–2771.
 (43) Zu, Y.; Fee, J. A.; Hirst, J. *J. Am. Chem. Soc.* **2001**, *123*, 9906–9907.

Scheme 1. Predominant Kinetic Pathway Proposed for the Oxidation of Ubiquinol by Excited-State $\text{Ru}(\text{bpy})_2(\text{pbim})^+ a$



^a Other possible pathways, including reactions of the ground-state first-order complex, are omitted for simplicity. Abbreviations: $(\text{L}_2)\text{Ru}(\text{II})(\text{pbim}^-)$ (**1**), deprotonated ground state; $(\text{L}_2)^-\text{Ru}(\text{III})(\text{pbim}^-)$ (**2**), deprotonated excited state; $(\text{L}_2)^-\text{Ru}(\text{III})(\text{pbim}^-)\text{---QH}_2$ (**3**), excited-state encounter complex; $(\text{L}_2)^-\text{Ru}(\text{II})(\text{pbimH})\text{---QH}^+$ (**4**), charge-separated state; $(\text{L}_2)^-\text{Ru}(\text{II})(\text{pbimH})$ (**5**), dissociated charge separated state; *, excited singlet state; QH_2 , quinol; QH^+ , neutral semiquinone; L, 2,2'-dipyridyl; pbim^- , 2-(2-pyridyl)benzimidazolate; pbimH , 2-(2-pyridyl)benzimidazole. In the excited state, **2** and **3**, fast equilibrium between the uncomplexed species, **2**, and QH_2 results in encounter complex formation, from which PCET reactivity (k_q) can occur. Electron transfer and coupled proton transfer produces a short-lived charge-separated state, **4**, within the encounter complex, which then rapidly diffuses into a solvent-separated radical pair. Charge recombination (k_{rec}) occurs via both first- and second-order processes to recycle the system back to the original ground-state mixture of mostly uncomplexed species. Note that the ground state (**1**) is also in hydrogen-bonding equilibrium with QH_2 ; this species is omitted for simplicity since its concentration is very small compared to that of **1** (see Results section).

of the Rieske $[\text{2Fe}_2\text{S}]$ center in the *cyt bc_1* complex to probe this unusual activation isotope effect in a system that exhibits unambiguous $n = 1$ electron- (and proton) transfer reactivity with $\text{UQH}_2\text{-0}$.

Experimental Section

Chemicals. All photochemical experiments were carried out in an $\text{Ar}(\text{g})$ atmosphere. Sodium sulfate, molecular sieves (4 Å), chloroform, chloroform- d_1 , acetonitrile- d_3 , 2,3-dimethoxy-5-methyl-1,4-benzoquinone, trimethyl-1,4-benzoquinol, 2,2'-bipyridyl, 1,2-diaminobenzene, picolinic acid, RuCl_3 , ammonium hexafluorophosphate, sodium borohydride, sodium borodeuteride, D_2O , and 30% DCl were obtained from Aldrich. The purity of trimethyl-1,4-benzoquinol, 2,3-dimethoxy-5-methyl-1,4-benzoquinol, and respective isotopomers was verified by ^1H NMR spectra. Acetonitrile (Aldrich) was dried over 4 Å molecular sieves before use. 2-(2-Pyridyl)benzimidazole (pbimH),⁴⁶ $\text{Ru}(\text{bpy})_2\text{Cl}_2 \cdot \text{H}_2\text{O}$,⁴⁷ and $\text{Ru}(\text{bpy})_2(\text{pbim})(\text{PF}_6)_2$ ⁴⁸ were prepared according to standard literature procedures. Details of the syntheses and characterization of the products can be found in the Supporting Information.

Preparation of Quinol Stocks. Ubiquinol-0 (2,3-dimethoxy-5-methyl-1,4-benzoquinol, $\text{UQH}_2\text{-0}$) and trimethylquinol (2,3,5-trimethyl-1,4-benzoquinol, TMQH_2), the primary reductants used in this study, differ from the biological substrates in that the latter have a 6-(isoprenyl) $_n$ tail used to maintain membrane solubility. The redox potentials of the two quinols are not substantially different, so we expect the use of $\text{UQH}_2\text{-0}$ to closely resemble the reactivity of $\text{UQH}_2\text{-10}$. $\text{UQH}_2\text{-0}$ stocks were freshly prepared before each experiment by sodium borohydride reduction in 1:1 acetonitrile:water followed by acidification

and extraction into a minimal volume of chloroform, which then was dried over Na_2SO_4 and diluted to an appropriate concentration with acetonitrile. $\text{UQD}_2\text{-0}$ (i.e., $\text{UQH}_2\text{-0}$ deuterated at its hydroxyl positions) was prepared using the same method but substituting deuterium oxide, sodium borodeuteride, and 30% DCl in D_2O . TMQD_2 was prepared from the protiated quinol by exchange with D_2O for 30 min under Ar followed by chloroform extraction and evaporation to dryness under an Ar stream. All isotope-dependent experiments reported involve the use of TMQD_2 and $\text{UQD}_2\text{-0}$ as the only isotopic preparations. Deuterium kinetic isotope effects are defined as $\text{KIE} = k_{\text{H}}/k_{\text{D}}$ for these experiments.

Time-Resolved Luminescence Decay Kinetics. Samples were prepared under Ar (g) and further deoxygenated by bubbling with ultrapure Ar (g) for 1 min prior to taking measurements. Excitation at 440 nm was provided by a frequency-tripled Q-switched Nd:YAG pumped optical parametric oscillator (Quantel Brilliant, OPOtech, Carlsbad, CA) with a pulse duration of approximately 10 ns. Luminescence was detected through a 635 nm interference filter (5 nm band-pass) by a photomultiplier (Hamamatsu, rise time 9 ns) protected from saturation by a neutral density filter. Second-order rate constants for QH_2 oxidation were obtained by Stern–Volmer titration, monitoring the emission decay lifetime of the complex. Because all data sets were well fit by first-order exponential decay curves, we assumed that the overall decay rate, k_{obs} , was the sum of two contributions: k_1 = the intrinsic rate of decay for luminescence in the absence of quenching by quinol and k_{ET} = the quenching rate from the reaction with QH_2 . The calculated second-order rate constant for the luminescence quenching by reaction with QH_2 was found to be independent of ground-state $\text{Ru}(\text{pbim})$ concentrations. An excess of QH_2 relative to $\text{Ru}(\text{pbim})$ was used in all experiments to ensure pseudo-first-order conditions with respect to QH_2 .

Time-Resolved Electron Paramagnetic Resonance (EPR). Laser pulses at 440 nm, as above, were directed onto a sample in the resonant cavity of a Bruker ESP 300e EPR spectrometer. The signal from the preamplifier output of the microwave bridge was amplified (1.5 ns rise time, Ortech model 9631, Oak Ridge, TN) and digitized at 10 ns time resolution (National Instruments model NI 5911, Austin, TX). Signals at a fixed magnetic field strength were averaged over 256–512 laser shots. Equivalent results were achieved whether the sample was flowed (approximately 0.3 mL min^{-1}) through a capillary cell (Bruker Aqua-X) or placed nonflowing in a flat cell ($\sim 0.3 \text{ mm}$ path length). Emission decay and cyclic voltammetry measurements performed on samples used in the TR-EPR experiment indicated very little sample degradation and practically no buildup of Q, a product of quinol and semiquinone auto-oxidation which might interfere with the measurement by oxidative quenching of $^3\text{Ru}(\text{pbim})$.

^1H NMR. Spectra were recorded on a Varian Mercury 300 MHz NMR spectrometer at the Washington State University Center for NMR spectroscopy. All experiments were performed at 19 °C in acetonitrile- d_3 . Samples were prepared in the usual manner and then completely dried under Ar (g) for dissolution in deuterated solvent.

Electrochemical Determination of pK_a Values in Acetonitrile. pK_a determinations were carried out as described by Kim and co-workers with slight modification.^{49,50} Details of the electrochemical apparatus and experimental procedure can be found in the Supporting Information.

Molecular Modeling and Computational Studies. Geometry optimization of the ground-state encounter complex between $\text{Ru}(\text{pbim})$ and UQH_2 were carried out using NWChem, at the B3LYP/DZVP level of theory.⁵¹ The 6-methyl analogue of $\text{UQH}_2\text{-0}$ was used in all models to preserve symmetry and avoid multiple structures. Modeling of the *cyt bc_1* Q_o pocket was performed using the crystal structure coordinates

(44) Ding, H.; Moser, C. C.; Robertson, D. E.; Tokito, M. K.; Daldal, F.; Dutton, P. L. *Biochemistry* **1995**, *34*, 15979–15996.

(45) Samoilova, R. I.; Kolling, D.; Uzawa, T.; Iwasaki, T.; Crofts, A. R.; Dikanov, S. A. *J. Biol. Chem.* **2002**, *277*, 4605–4608.

(46) Ayers, T.; Caylor, N.; Ayers, G.; Goodwin, C.; Hathcock, D.; Stutman, V.; Slatterly, S. J. *Inorg. Chim. Acta* **2002**, *328*, 33–38.

(47) Sullivan, P.; Salmon, D. J.; Meyer, T. J. *Inorg. Chem.* **1978**, *17*, 3334–3341.

(48) Haga, M.-A. *Inorg. Chim. Acta* **1983**, *75*, 29–35.

(49) Kim, H. S.; Chung, T. D.; Kim, H. J. *Electroanal. Chem.* **2001**, *498*, 209–215.

(50) Kim, J.; Chung, T. D.; Kim, H. J. *Electroanal. Chem.* **2001**, *499*, 78–84.

(51) High Performance Computational Chemistry Group, N., *A Computational Chemistry Package for Parallel Computers*, version 4.0.1; Pacific Northwest National Laboratory: Richland, WA, 1998.

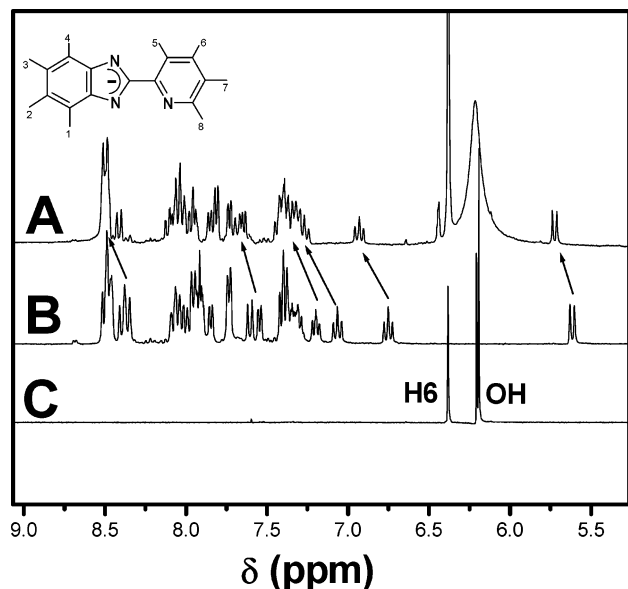


Figure 1. ^1H NMR spectrum (300 MHz, acetonitrile- d_3) of (A) a mixture of **1** (5 mM) and UQH₂-0 (>50 mM), (B) 5 mM **1** alone, and (C) UQH₂-0 (40 mM).

of bovine cyt *bc*₁ (PDB file 1PPJ)⁵² with bound stigmatellin, using the optimized structure of 6-methyl-UQH₂-0 as a model for the UQH₂-10 substrate.

Results

Ubiquinol Hydrogen Bonds to the Benzimidazolate Ligand, pbim, in a Transient Ground-State Encounter Complex.

Figure 1A shows that the ^1H NMR spectrum of superstoichiometric UQH₂-0 (50 mM) with **1** (5 mM) exhibited downfield shifts in the benzimidazolate proton signals of the pbim ligand compared with that of complex alone (Figure 1B) and a broadening of UQH₂-0 hydroxyl proton signals. (See Scheme 1 for identification of the chemical species.) Acetonitrile- d_3 was used as a solvent in these measurements for consistency with the optical and EPR measurements. Benzimidazolate ($\delta = 5.61$ (H₁), 6.74 (H₂), 7.06 (H₃), and 7.60 (H₄) ppm; unshifted) and pyridine ($\delta = 8.45$ (H₇), 7.84 (H₈), 7.54 (H₅), and 7.19 (H₆) ppm; unshifted) ring proton signals all exhibited downfield shifts upon UQH₂-0 addition. The observed shifts were intermediate between those of the deprotonated form of the complex, **1**, and its protonated form (see Supporting Information), Ru(pbimH)²⁺, implying a hydrogen-bonding interaction between UQH₂-0 and the pbim ligand. No other large changes were observed for signals associated with the bipyridyl ligands, suggesting the effect to be localized to the pbim ligand. Figure 1C shows a spectrum of authentic UQH₂-0, allowing the peaks in Figure 1C and A at $\delta = 6.38$ and 6.21 to be attributed to H6 and the hydroxyl protons, respectively, of UQH₂-0. The dissociation constant between UQH₂-0 and **1** was not obtainable from these NMR experiments because of significant protonation of the Ru complex by acidic impurities, which occurred at very high concentrations of **1** (>10 mM) and UQH₂-0 (>50 mM) near the lower bounds required for determining the dissociation constant.

The absence of an optical absorbance change in the NMR samples in the 490 nm shoulder of the MLCT absorption band

upon UQH₂-0 addition (data not shown) ruled out the possibility of a large (favorable) equilibrium constant for proton exchange between UQH₂-0 and **1**. We also note that photochemistry was unlikely to have been responsible for the observed NMR shifts since the sample was maintained in the dark.

Emission Quenching of Excited-State Ru(pbim) Occurs by a Proton-Linked Electron-Transfer Mechanism. The inset of Figure 2A shows that, at 23 °C, titration of UQH₂-0 in the 1–13 mM range quenched luminescence from the excited triplet state of Ru(pbim)⁺, species **2** (Scheme 1), the rate of which was approximately linear with [UQH₂-0]. Furthermore, the luminescence decay kinetics were well fit by first-order exponential curves, indicating that the reaction of UQH₂-0 with **2** was pseudo-first order with respect to UQH₂-0. No changes were observed in the amplitude of the emission decay curves when extrapolated to the time of the activating flash as long as **2** remained in the deprotonated state prior to reaction, showing that the addition of UQH₂-0 did not alter the intrinsic photochemical properties of the complex. The linear luminescence quenching plot, Figure 2A (inset), is assigned to ET quenching of the luminescent MLCT state of **2** within a diffusional ‘Marcus-type’ precursor complex (see NMR data above). The calculated second-order rate constant for quenching by UQH₂-0 was $4.3 \times 10^7 \text{ M}^{-1} \text{ s}^{-1}$. The rate constant for quenching by UQH₂-0 was >10-fold smaller for the conjugate acid of **2**, even though the estimated excited-state redox potential of this species is expected to be 110 mV higher than its deprotonated form,⁴⁸ which would suggest a much higher rate if the electron transfer were not coupled to proton transfer (PT). The simplest interpretation of this data is that the most rapid route for ET quenching involves hydrogen bonding of UQH₂ to **2** (to form species **3** in Scheme 1) followed by proton and electron transfer, as expected given the large ground-state ΔpK_a and redox-associated pK_a shifts for both reactants.^{6,48,53}

Deuterium Kinetic Isotope Effects. Ubiquinol deuterated at the 1,4-hydroxyl positions, UQD₂-0, reacted with **2** in a manner similar to its protiated form but with a rate constant of $2.3 \times 10^7 \text{ M}^{-1} \text{ s}^{-1}$ (see Figure 2A). Consistent with the UQH₂-0 results, the rate of UQD₂-0 quenching decreased by >10-fold when protonated **2** was used as an oxidant. The average KIE was 1.87 at 23 °C, consistent with a PCET reaction.^{54,55} TMQH₂-0, an analogue of plastoquinol, gave similar results to that of UQH₂-0 (Figure 2B (inset)), exhibiting second-order rate constants of 6.9×10^7 and $2.0 \times 10^7 \text{ M}^{-1} \text{ s}^{-1}$ for protiated and deuterated isotopomers, respectively (KIE = 3.45 at 23 °C).

Figure 2 also demonstrates that both the protiated and deuterated forms of UQH₂-0 exhibited reasonably linear Arrhenius plots over the temperature range of 3–40 °C. We estimated an Arrhenius activation free energy, ΔG^{TS} , for luminescence quenching by UQH₂-0 oxidation, $\Delta G^{\text{TS}}(\text{H})$, of $36.3 \pm 1.6 \text{ kJ mol}^{-1}$ with a preexponential term, $A(\text{H})$ of $8.9 \times 10^{13} \text{ M}^{-1} \text{ s}^{-1}$. Surprisingly, oxidation of UQD₂-0 gave a substantially lower activation barrier, $\Delta G^{\text{TS}}(\text{D}) = 24.4 \pm 2.3 \text{ kJ mol}^{-1}$ with $A(\text{D}) = 5.8 \times 10^{11} \text{ M}^{-1} \text{ s}^{-1}$ than did the protiated form. The qualitative observation of $\Delta G^{\text{TS}}(\text{H}) > \Delta G^{\text{TS}}(\text{D})$ was

(53) Roginsky, V. A.; Pisarenko, L. M.; Bors, W.; Michel, C. *J. Chem. Soc., Perkin Trans. 2* **1999**, 871–876.

(54) Decornez, H.; Hammes-Schiffer, S. *J. Phys. Chem. A* **2000**, *104*, 9370–9384.

(55) Mayer, J. M.; Hrovat, D. A.; Thomas, J. L.; Borden, W. T. *J. Am. Chem. Soc.* **2002**, *124*, 11142–11147.

(52) Huang, L.; Cobessi, D.; Crofts, A. R.; Berry, E. A. Manuscript in preparation.

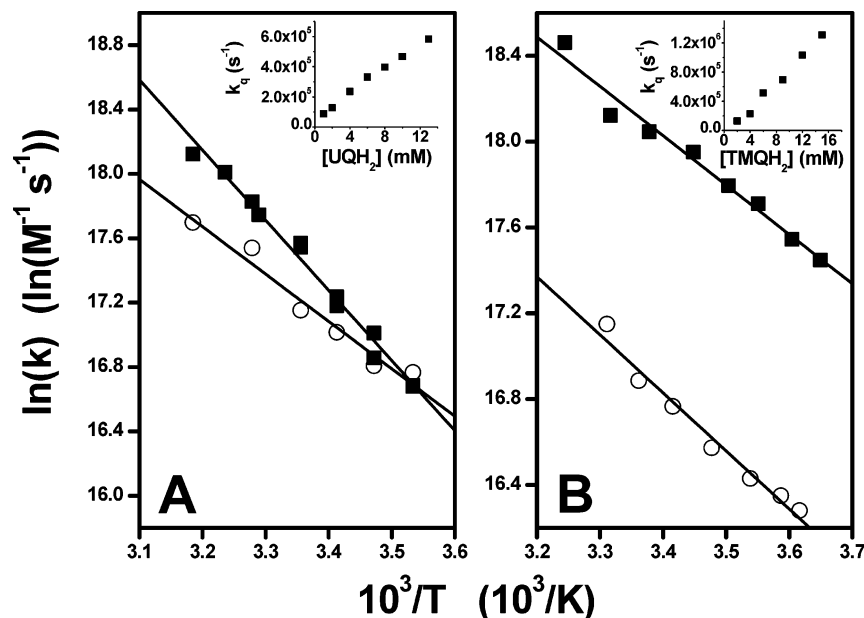


Figure 2. Arrhenius plots of (A) UQH₂-0 (closed squares) and UQD₂-0 (open circles) oxidation and (B) TMQH₂-0 (closed squares) and TMQD₂-0 (open circles) oxidation by **2** in acetonitrile. (Insets) Luminescence quenching titrations for UQH₂-0 and TMQH₂-0.

highly reproducible between different preparations of QH₂ and **1** as well as different batches of solvent as long as the solvent was scrupulously dried, and thus, we conclude that the effect is not a result of impurities in one of the isotopic preparations or the solvent. As discussed below, the smaller ΔG^{TS} for the deuterated quinol is contrary to expectations from traditional treatments of primary KIE's⁵⁶ but was qualitatively similar to that seen in biological UQH₂-10 oxidation.³⁴

In contrast to the observations for UQH₂-0/UQD₂-0 oxidation, the activation parameters found for the oxidation of the plastoquinol analogue TMQH₂-0 (see Figure 2B) were consistent with semiclassical theoretical considerations;⁵⁶ Arrhenius activation parameters for oxidation of TMQH₂-0 were $\Delta G^{\text{TS}}(\text{H}) = 19.1 \pm 1.2$ kJ/mol and $A(\text{H}) = 1.7 \times 10^{11}$ M⁻¹ s⁻¹, while for TMQD₂-0 $\Delta G^{\text{TS}}(\text{D}) = 22.3 \pm 1.5$ kJ/mol and $A(\text{D}) = 2.0 \times 10^{11}$ M⁻¹ s⁻¹. Again, this behavior is qualitatively similar to that observed for the cyt *bc*₁ complex, where plastoquinol substitution for UQH₂ eliminated the unusual isotope effect on ΔG^{TS} .

Proton-Transfer Equilibria. The pK_a values for ground-state, protonated, **1** and UQH₂-0 in acetonitrile were estimated, as described by Kim and co-workers,^{49,50} from acid-induced shifts in the reductive wave (E_c) of the benzoquinone/benzo-semiquinone couple. UQH₂-0 and **1**, under the solvent conditions used in our kinetic assays (23 °C), were estimated to have pK_a values of ca. 25.5 and 17.9, respectively, giving $\Delta G_{\text{PT}}^{\circ} \approx 43.3$ kJ/mol.

Time-Resolved EPR Demonstrates a Neutral Ubisemiquinone Intermediate upon UQH₂-0 Oxidation. Time-resolved direct-detection electron paramagnetic resonance (TR-EPR) was employed to probe the intermediate species formed in the photoinduced oxidation of UQH₂-0. A radical species, centered at $g = 2.006$, was observed (Figure 3A–C) with well-defined proton hyperfine splittings, consistent with the CW-EPR spectra of other neutral ubisemiquinone species.⁵⁷ A quartet

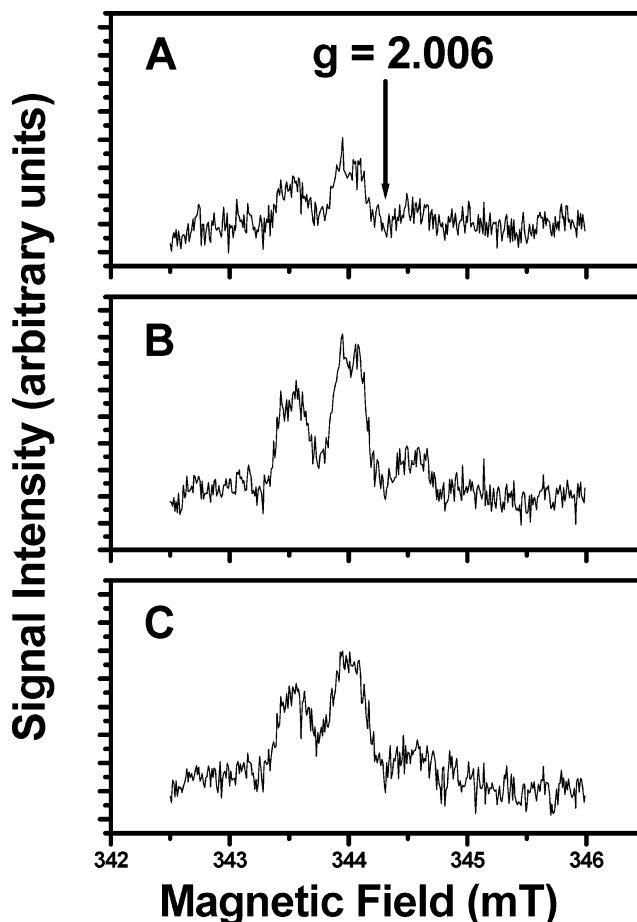


Figure 3. Time-resolved EPR spectra of the semiquinone intermediate formed during UQH₂-0 oxidation by **2** (5 mM ground-state concentration). Spectra were taken (A) 160, (B) 480, and (C) 960 ns after excitation.

of hyperfine splittings ($A = 4.95$ G) is observed in the spectrum (Figure 3B) and is attributable to the 5-methyl protons of the

(56) Bell, R. P. *The Tunnel Effect in Chemistry*; Chapman and Hall: New York, 1980.

(57) In *CRC Handbook of EPR Spectra from Quinones and Quinols*; Pederson, J. A., Ed.; CRC Press Inc.: Boca Raton, FL, 1985.

neutral ubisemiquinone radical. A poorly resolved doublet splitting ($A = 1.35$ G) is attributable to the 6-H position. The very small splittings expected from the 2- and 3-methoxy protons are not resolved in the spectrum, as is usual for most CW-EPR spectra of ubisemiquinone species. The observed hyperfine splittings conclusively show that the radical is the neutral semiquinone UQH^\bullet and not $\text{UQ}^{\bullet-}$ or $\text{UQH}_2^{\bullet+}$. It should be noted that the other radical formed in these reactions, a ligand-centered radical on the bipyridyl ligands of the reduced ruthenium species, **4** and **5**, is rarely observed in EPR measurements of ruthenium polydiimine complexes due to intramolecular exchange broadening (ligand hopping).⁵⁸

The TR-EPR spectra exhibited a large distortion in the amplitude of the hyperfine-shifted peaks away from the 1:3:3:1 ratio for the quartet of a methyl proton hyperfine pattern. This distortion was not caused by progressive breakdown of the sample since neither flowing the sample nor changing the field sweep direction affected the spectral shape. In addition, across the spectrum the radicals emit microwaves rather than absorbing them. The emission and asymmetry result from a mixture of chemically induced dynamic electron polarization (CIDEP) effects, specifically a triplet mechanism (TM), or triplet mechanism-like, polarization and radical pair mechanism (RPM) polarization effects.^{59,60} TM, or TM-like, polarization accounts for the net emissive character of the spectra in Figure 3, while RPM polarization accounts for the asymmetry between the high- and low-field portions of the spectrum. The triplet sublevels of the photoexcited ruthenium polypyridyl complex reach thermal equilibrium on the picosecond time scale because of the rapid spin–lattice relaxation at the Ru(III) center in the MLCT state. Thus, the normal TM would not produce any spin polarization. However, recombination in the contact radical pair, species **4** (Scheme 1), consisting of the oxidized quinol and reduced ruthenium complex, involves intersystem crossing which can selectively deplete radical pair triplet sublevels. The TM-like polarization observed here apparently results from such spin-selective recombination of the contact radical pair state.^{61,62}

Another notable feature of the spectrum is that it shows no sign of correlated radical pair polarization (CRP) in which one side of each line in the spectrum is emissive and the other side is absorptive.^{63,64} CRP can result from a reaction from a triplet state, as here, but requires that the product radicals continue to interact with each other, i.e., in close proximity, in contact, or connected to each other. The absence of CRP in this case indicates that the SQ radical does not remain hydrogen bonded to the ruthenium complex, as in species **4**, but diffuses rapidly away before the first EPR signals are observed to form species **5**. Re-encounters during this initial separation provide opportunities for recombination of the radicals, producing the observed RPM polarization contribution to the spectrum. Thus, these EPR measurements indicate that quenching involves transfer of an electron and a proton from the QH_2 to the

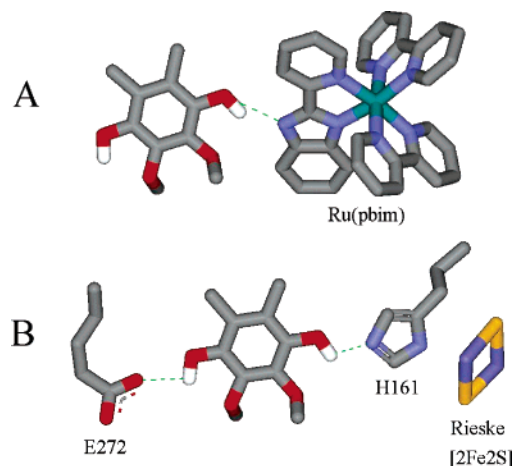


Figure 4. Model structures of UQH_2 (A) in an encounter complex with **1**, optimized at the B3LYP/DZVP level of theory and (B) bound in the Q_0 pocket of the cyt bc_1 complex, modified from PDB ID: 1PPJ.⁵² Color scheme: oxygen, red; carbon, gray; nitrogen, blue; hydrogen, white; sulfur, yellow; iron, lavender; ruthenium, turquoise. See text for modeling details.

photoexcited MLCT state of the Ru complex followed by separation of the QH^\bullet and **5** before eventual recombination of the radicals to regenerate the starting compounds.

It is not possible to estimate the rate constants or SQ yield from the current EPR data alone due to the fact that the radical formation kinetics are convoluted with the electron spin dynamics observed by TR-EPR. However, there is no lag in the appearance of the SQ signal, and no other signals were observed at early times after laser excitation, suggesting that the SQ species in Figure 3 is the first and only quasi-stable intermediate. Preliminary spectra recorded using different quinol substrates exhibited different splitting patterns consistent with their SQ states, demonstrating that the spectrum obtained is indeed due to quinol oxidation.

Discussion

Encounter Complex. ^1H NMR spectra of ground-state **1** and $\text{UQH}_2\text{-}0$ in acetonitrile- d_3 (Figure 1) indicates a hydrogen-bonding interaction between the reactants. The formation of this complex is characterized by broadening of the $\text{UQH}_2\text{-}0$ hydroxyl proton resonances and downfield shifts of the benzimidazolone proton resonances. These features of complex formation are similar to spectra of quinone-binding moieties in more strongly bound complexes.^{65–68} We suggest that this transient complex is similar to the encounter complex formed in the excited-state reaction.

We modeled the **1**– $\text{UQH}_2\text{-}0$ ground-state hydrogen-bonded complex in the gas phase using density functional theory calculations at the B3LYP/DZVP level of theory to determine if the interaction observed in the ^1H NMR spectra discussed above (see Figure 4A) is conducive to proton transfer. In line with this hypothesis, the minimized structure revealed a hydrogen bond between the $\text{UQH}_2\text{-}0$ hydroxyl proton and the deprotonated benzimidazolone of the pbim ligand. The heavy-

(58) Samuels, A. C.; DeArmond, M. K. *Inorg. Chem.* **1995**, *34*, 5548–5551.

(59) Pederson, J. B.; Freed, J. H. *J. Chem. Phys.* **1973**, *58*, 2746–2762.

(60) Jager, M.; Norris, J. R., Jr. *J. Magn. Reson.* **2001**, *150*, 26–34.

(61) Tero-Kubota, S.; Katsuki, A.; Korbori, Y. *J. Photochem. Photobiol. C: Photochem. Rev.* **2001**, *2*, 17–33.

(62) Morozova, O. B.; Tsentelovich, Y. P.; Yurkovskaya, A. V.; Sagdeev, R. *Z. Chem. Phys. Lett.* **1995**, *246*, 499–505.

(63) Closs, G. L.; Forbes, M. D.; Norris, J. R. *J. Phys. Chem.* **1987**, *91*, 3592–3599.

(64) Hasharoni, K.; Levanon, H.; Tang, J.; Bowman, M. K.; Norris, J. R.; Gust, D.; Moore, T. A.; Moore, A. L. *J. Am. Chem. Soc.* **1990**, *112*, 6477–6481.

(65) Chang, C. J.; Brown, J. D. K.; Chang, M. C. Y.; Baker, E. A.; Nocera, D. G. In *Electron Transfer in Chemistry*; Balzani, V., Ed.; Wiley-VCH: Weinheim, Germany, 2001; Vol. 2, pp 409–461.

(66) Kirby, J. P.; Roberts, J. A.; Nocera, D. G. *J. Am. Chem. Soc.* **1997**, *119*, 9230–9236.

(67) Prasad, E.; Godipas, K. R. *J. Am. Chem. Soc.* **2000**, *122*, 3191–3196.

(68) Hayashi, T.; Miyahara, T.; Koide, N.; Kato, Y.; Masuda, H.; Ogoshi, H. *J. Am. Chem. Soc.* **1997**, *119*, 7281–7290.

atom (O–N) distance was 2.89 Å, indicating that the hydrogen bond is of weak to moderate strength in the gas phase. The ground-state hydrogen-bond distance would likely increase in solution. This is consistent with the observed second-order reaction between quinol species and **2** in solution (see Figure 2).

It is important to note that no crystallographic data on UQH₂ bound to the Q_o site in cyt *bc*₁ has been reported, preventing a direct structural comparison of the bimolecular complex discussed here and the UQH₂ bound in the Q_o pocket. Our current structural view of the reactive enzyme–substrate complex (see Figure 4) is based almost exclusively on the binding of a quinone analogue, stigmatellin, which is a very strong inhibitor of the Q_o site. Stigmatellin forms moderate strength hydrogen bonds on either side of its chromone ring with histidine 161, a ligand to the Rieske 2Fe2S center, and glutamate 272 on the cyt *b* subunit. H161 is thought to be the initial proton acceptor to QH₂ in the Q_o pocket,^{69,70} while the function of E272, beyond a simple structural feature and possible proton conduit,^{24,71,72} is currently not resolved. In contrast to stigmatellin, substrate UQH₂ apparently binds less tightly (and is lost during crystallization) and thus likely possesses much weaker hydrogen bonds than stigmatellin. When UQH₂ was modeled in the same position as stigmatellin (Figure 4), it formed two hydrogen bonds with H161 and E272 with average heavy-atom distances of 3.03 Å, consistent with previous proposals.^{9,24,26,71,72} Thus, the hydrogen bond of functional significance, between quinol and the deprotonated histidine, in the proposed enzyme–substrate complex and biomimetic system, is reasonably similar, at least within these substantial ambiguities.

Sequential PT-ET vs PCET Models of Reactivity. From our estimate of pK_a values for UQH₂-0 and ground-state **1**^{49,50} in acetonitrile we estimate $\Delta G^{\circ}_{\text{PT}}$ to be ~43.3 kJ/mol. As previously argued for similar systems,^{55,73,74} the observed activation energies in both isotopomers of UQH₂-0 and TMQH₂ are too low (by ~6.7 and 24.2 kJ/mol for UQH₂ and TMQH₂, respectively) to be consistent with a preequilibrium proton-transfer step. Additionally, Haga and co-workers reported that **1** exhibits weak photoacidity in water, which, if also true in acetonitrile, would further increase $\Delta G^{\circ}_{\text{PT}}$ well above the observed activation energies.⁴⁸ Likewise, an ET first pathway can be ruled out since the energy of formation of the intermediate quinol cation state, estimated by cyclic voltametry,⁷⁵ would be too endothermic by a minimum of 39 kJ/mol. We thus propose that the oxidation of UQH₂-0 occurs via a PCET mechanism (see Scheme 1).

Nature of the Unusual Isotope Effect on the Arrhenius Activation Barrier. Our data suggests that isotopic substitution to the UQH₂-0 hydroxyl groups results in a fundamentally different enthalpic barrier for electron/proton transfer in formation of the neutral semiquinone state. Qualitatively similar effects have now been observed for QH₂ oxidation in three different

reaction systems,^{34,36} all involving ubiquinol oxidation, in three different solvent environments (acetonitrile, ethanol,³⁶ and in the Q_o site of the cyt *bc*₁ complex³⁴), suggesting that the unusual isotope effect is an intrinsic and apparently specific feature of UQH₂ chemistry relative to other quinol substrates. In addition, similar isotope effects have been observed for non-quinol systems.^{11,37–40}

In contrast to the ruthenium and cyt *bc*₁ based UQH₂ oxidation studies, Nagaoka and co-workers³⁶ observed a large KIE (>21) in their system using α -tocopheryl radical as an oxidant for UQH₂ and a strongly negative value for $\Delta G^{\text{TS}}_{\text{D}} - \Delta G^{\text{TS}}_{\text{H}}$ (~5 kJ/mol, resulting in a ~50% decrease in the slope of their UQD₂ Arrhenius plot compared with UQH₂) and attributed this observation to tunneling. However, with a tunneling mechanism one generally expects nonnegative values for $\Delta G^{\text{TS}}_{\text{D}} - \Delta G^{\text{TS}}_{\text{H}}$, suggesting that additional factors may explain the presence of a negative $\Delta G^{\text{TS}}_{\text{D}} - \Delta G^{\text{TS}}_{\text{H}}$ in their results. We suggest three explanations for these observations: (1) equilibrium isotope effects on hydrogen bonding or PT equilibria, (2) kinetic complexity involving competition between PCET and sequential PT/ET reactions, and (3) the possibility of transition-state dynamics. Thus far, we have only observed strongly negative $\Delta G^{\text{TS}}_{\text{D}} - \Delta G^{\text{TS}}_{\text{H}}$ with *o*-methoxy quinols (decyl-UQH₂ in the enzyme and UQH₂-0 in the present biomimetic system), possibly suggesting an important role for intramolecular hydrogen bonding in the reaction mechanism, as suggested by de Heer and co-workers.⁷⁶ Assays with a larger range of substituted quinols might resolve this issue. Finally, although it appears that the presence of a negative value for $\Delta G^{\text{TS}}_{\text{D}} - \Delta G^{\text{TS}}_{\text{H}}$ is not dictated by the protein environment, the difference in magnitudes of $\Delta G^{\text{TS}}_{\text{D}} - \Delta G^{\text{TS}}_{\text{H}}$ (~10 kJ/mol) between the system discussed here and our studies on the cyt *bc*₁ complex could indicate some contribution from the protein to the magnitude of the effect.

How Does the Q_o Pocket Influence the Oxidation of QH₂? Villa and Warshel⁷⁷ and Doll and Finke⁷⁸ suggested that to truly understand the mechanism of an enzymatically catalyzed reaction we must first understand the mechanism of the nonenzymatic reaction. This has been the basic approach of the present work. The overall conclusion we reach is that despite its simplicity with respect to the enzyme (a smaller number of potential hydrogen bonds, lack of protein vibrational modes, etc.), the biomimetic system can reproduce key features of the oxidative process, including the activation isotope effects and their sensitivity to QH₂ ring substituents. The simplest interpretation is that the reaction coordinates are not radically different between the Q_o site and the biomimetic systems, outside of the obvious differences in dielectric constant and driving forces. Our results thus support Type I rather than Type II mechanisms and provide a simple model system with which to study the rate-limiting reactions of the complicated cytochrome *bc*₁ complex.

Acknowledgment. This work was supported by the National Institutes of Health, GM61904 (M.K.B.), and U.S. Department of Energy, DE-FG03-98ER20299 (D.M.K.). The authors thank Drs. James Hurst, William Davis, James Mayer, William Parson,

(69) Esser, L.; Quinn, B.; Li, Y. F.; Zhang, M.; Elberry, M.; Yu, L.; Yu, C. A.; Xia, D. *J. Mol. Biol.* **2004**, *341*, 281–302.

(70) Xia, D.; Esser, L.; Singh, S. K.; Guo, F.; Maurizi, M. R. *J. Struct. Biol.* **2004**, *146*, 166–179.

(71) Crofts, A. R.; Hong, S.; Ugulava, N.; Barquera, B.; Gennis, R.; Guergova-Kuras, M.; Berry, E. A. *Proc. Natl. Acad. Sci.* **1999**, *96*, 10021–10026.

(72) Hunte, C.; Palsdottir, H.; Trumppower, B. L. *FEBS Lett.* **2003**, *545*, 39–46.

(73) Mayer, J. M. *Annu. Rev. Phys. Chem.* **2004**, *55*, 363–390.

(74) Roth, J. P.; Yoder, J. C.; Won, T.-J.; Mayer, J. M. *Science* **2001**, *294*, 2524–2526.

(75) Cauquis, G.; Marbach, G. *Biochim. Biophys. Acta* **1972**, *283*, 239–246.

(76) de Heer, M. I.; Korth, H.-G.; Mulder, P. *J. Org. Chem.* **1999**, *64*, 6969–6975.

(77) Villa, J.; Warshel, A. *J. Phys. Chem. B* **2001**, *105*, 7887–7907.

(78) Doll, K. M.; Bender, B. R.; Finke, R. G. *J. Am. Chem. Soc.* **2003**, *125*, 10877–10884.

Sharon Hammes-Schiffer, Mikial Vener, and Arieh Warshel for stimulating discussions. Part of this work was performed at the WR Wiley Environmental Molecular Sciences Laboratory, a national scientific user facility sponsored by the Department of Energy's Office of Biological and Environmental Research and located at Pacific Northwest National Laboratory.

Supporting Information Available: Details of the syntheses, spectroscopic characterization, and electrochemistry. This material is available free of charge via the Internet at <http://pubs.acs.org>.

JA043955G